Geophysical Research Letters

RESEARCH LETTER
10.1029/2025GL119099

Special Collection:
SAGE Data Products: Algorithms, Science, and Applications for Upper Troposphere and Stratosphere Studies

Large Particle Size and Thick Coating Influence Pyrocumulonimbus Smoke Radiative Forcing and Stratospheric Warming: Insights From the 2019–2020 Australian Megafires

Xi Chen[1,2], Jun Wang[1,2], David A. Peterson[3], Yaowei Li[4,5], William Julstrom[1,2], Frank N. Keutsch[4,6,7], and John Dykema[4]

[1]Department of Chemical & Biochemical Engineering, The University of Iowa, Iowa City, IA, USA, [2]Center for Global and Regional Environmental Research, and Iowa Technology Institute, The University of Iowa, Iowa City, IA, USA, [3]Naval Research Laboratory, Monterey, CA, USA, [4]Paulson School of Engineering and Applied Sciences, Harvard University, Cambridge, MA, USA, [5]Now at Department of Earth, Atmospheric, and Planetary Sciences, Massachusetts Institute of Technology, Cambridge, MA, USA, [6]Department of Chemistry and Chemical Biology, Harvard University, Cambridge, MA, USA, [7]Department of Earth and Planetary Sciences, Harvard University, Cambridge, MA, USA

Abstract Large particle size and thick coatings have been detected in pyrocumulonimbus (pyroCb) smoke injected into the lower stratosphere, enhancing both extinction and absorption of smoke. Here, we quantified how particle size and coating, via internal mixing of non-absorbing species on black carbon, influence pyroCb smoke radiative forcing and stratospheric heating using core-shell Mie calculations coupled with chemical transport and radiative transfer models. Airborne measurements indicate a number median radius of 0.25 μm for days-old pyroCb smoke, larger than typical lower tropospheric smoke. This larger size approximately doubles aerosol extinction and enhances shortwave radiative forcing at the top of the atmosphere by 35%–60%, more consistent with satellite-observed radiative fluxes following 2019–2020 Australian pyroCb event. Coating enhances stratospheric heating by 1–1.5 K, twice the enhancement caused by larger particle size, yielding better agreement with stratospheric temperature anomaly observed from satellite during the first 3 months after injection.

Plain Language Summary Pyrocumulonimbus (pyroCb) plumes from intense wildfires injected large amount of biomass burning smoke particles into upper troposphere and lower stratosphere. Unlike the sulfate particles in the background stratosphere primarily scattering sunlight back to space, the black carbon (BC) in smoke strongly absorbs solar radiation, leading to different and even opposite radiative effects on Earth's energy budget. Thick coatings of non-absorbing species on BC cores were detected in most pyroCb particles from airborne measurements, which implies the larger particle size and enhanced absorption compared to smoke close to the surface. In this study, models are combined to quantify how large particle size and coating influence the pyroCb smoke radiative effect and stratospheric temperature perturbations. Satellite measurements after the 2019–2020 Australian pyroCb event are compared with model results. Large particle size was found to enhance the atmospheric opacity caused by smoke by 100% and scatter 35%–60% more sunlight back to space, reducing the downward radiation. Additionally, the enhanced absorption of coated pyroCb smoke can cause further 1–1.5 K heating in the stratosphere, agreeing with the satellite observed temperature anomalies. Our study demonstrates the significance of considering large size and coating of pyroCb smoke when evaluating the impact of pyroCb smoke on climate.

Key Points:

- The number median radius of days-old pyroCb smoke reaches 0.25 μm, larger than smoke in the boundary layer with radius smaller than 0.1 μm
- Larger pyroCb smoke size doubles the extinction and enhances shortwave radiative forcing at the top of the atmosphere by 35%–60%
- Coatings of pyroCb smoke enhance the stratospheric warming by 1–1.5 K through internal mixing, twice the effect of larger particle alone

Supporting Information:

Supporting Information may be found in the online version of this article.

Correspondence to:

X. Chen and J. Wang,
xi-chen-4@uiowa.edu;
jun-wang-1@uiowa.edu

Citation:

Chen, X., Wang, J., Peterson, D. A., Li, Y., Julstrom, W., Keutsch, F. N., & Dykema, J. (2026). Large particle size and thick coating influence pyrocumulonimbus smoke radiative forcing and stratospheric warming: Insights from the 2019–2020 Australian megafires. *Geophysical Research Letters*, *53*, e2025GL119099. https://doi.org/10.1029/2025GL119099

Received 3 SEP 2025
Accepted 23 MAR 2026

Author Contributions:

Conceptualization: Xi Chen, Jun Wang, David A. Peterson

1. Introduction

The potential impacts of fire-generated thunderstorms, known as pyrocumulonimbus (pyroCb), on atmosperhic compositon and climate prediction have been recognized since the early 2000s (M. Fromm et al., 2000; M. D. Fromm & Servranckx, 2003). Driven by dry air near the surface, which nurtures vigorous fire activity and abundant moisture several kilometers above, pyroCb injection can reach the upper troposphere and lower stratosphere (UTLS) (Peterson et al., 2017, 2021). PyroCb plumes not only contain many cloud droplets and ice particles, but also inject abundant biomass-burning smoke particles into the UTLS, with a mass comparable to that of sulfate particles associated with a moderate volcanic eruption (Peterson et al., 2018). Multi-year airborne

Data curation: Xi Chen, Yaowei Li, William Julstrom, Frank N. Keutsch, John Dykema
Formal analysis: Xi Chen
Funding acquisition: Jun Wang, David A. Peterson
Investigation: Xi Chen, William Julstrom
Methodology: Xi Chen, David A. Peterson
Project administration: Jun Wang, David A. Peterson
Resources: Jun Wang, Yaowei Li, Frank N. Keutsch, John Dykema
Software: Xi Chen
Supervision: Jun Wang, David A. Peterson
Validation: Xi Chen
Visualization: Xi Chen
Writing – original draft: Xi Chen
Writing – review & editing: Xi Chen, Jun Wang, David A. Peterson, Yaowei Li, Frank N. Keutsch, John Dykema

observations demonstrated that these pyroCb smoke particles account for 10%–25% of the black carbon (BC) and organic aerosols in the "present-day" lower stratosphere, which is viewed traditionally to be dominated by sulfate particles (Katich et al., 2023).

It is critical to understand how these smoke particles in the UTLS may affect the energy balance of the climate system, since BC in smoke particles strongly absorbs solar radiation unlike sulfate particles with strong scattering. Christian et al. (2019) indicates that this BC absorption can exceed the reflective effect of organic carbon (OC) in smoke and cause a net instantenous positive shortwave (SW) radiative forcing (RF) at the top of the atmosphere (TOA), opposite to the cooling effect from stratospheric sulfate (Andersson et al., 2015; Ge et al., 2016; Ridley et al., 2014; Solomon et al., 2011). However, pyroCb events differ not only in injection heights, but also in smoke optical properties (Sellitto et al., 2022) determined by smoke composition (BC fraction) and particle size, both of which substantially influencing pyroCb smoke RF estimates (Heinold et al., 2022; Li et al., 2021; Wang et al., 2006). Additionally, the dominant absorption of both SW and longwave radiation by aerosols in the UTLS typically exceeds the enhanced longwave cooling due to aerosol-caused stronger emissivity, resulting in net radiative heating in the UTLS (Robock, 2000). Hence, pyroCb smoke is hypothesized to heat the UTLS, similar to volcanic sulfate, whereas the heating rate (HR) may be different from sulfate given stronger SW absorption of smoke.

This study quantifies the impact of pyroCb smoke particle size and coating on RF and stratospheric warming through a hybrid observational and modeling approach. Previous measurements of wildfire smoke collected in the lower troposphere (LT) or boundary layer have illustrated that most biomass burning smoke is internally mixed where BC particles are coated by non-absorbing shells (e.g., Martins et al., 1998; Reid & Hobbs, 1998; Reid et al., 2005; Taylor et al., 2020). This coating was also found to significantly enhance the absorption of smoke particles compared to those externally mixed particles less frequently detected in smoke (Lack et al., 2012; Martins et al., 1998). The different mixing states of BC-containing urban aerosols can also cause as much as 60% difference in aerosol optical depth (AOD) retrieval from satellite (Wang & Martin, 2007). Consequently, a higher positive direct RF from BC than previously thought was assessed due to coating, highlighting the greater significance of BC in global climate warming (Jacobson, 2001). Although the impact of coating on BC particles in the smoke on their direct RF has been comprehensively evaluated (Wang & Christopher, 2006), the potential coating of OC and background sulfate in the UTLS on BC in pyroCb smoke, as well as its impact on pyroCb RF and stratospheric heating is not well constrained.

Recent airborne measurements have shown that the properties of pyroCb smoke particles in the UTLS are different from that of LT smoke. For instance, stronger aerosol extinction and larger particle size of smoke particles were observed in a recent field experiment detecting freshly injected pyroCb of hours-age (Peterson et al., 2022), compared with those reported for LT smoke from similar biomass burning (volume geometric mean diameter of 0.27–0.29 μm vs. 0.1–0.16 μm) (e.g., Reid et al., 2005; Alonso-Blanco et al., 2012; Portin et al., 2012). The large mode of volume size distribution of pyroCb smoke particles aged for several days in 0.5–0.6 μm diameter was detected in the 2022 Dynamics and Chemistry of the Summer Stratosphere (DCOTSS) airborne mission (Li et al., 2025). Most BC particles in elevated smoke plumes in the lowermost stratosphere exhibited much larger coating thickness than fresh LT smoke, as large as 255 nm (Dahlkötter et al., 2014; Katich et al., 2023). Similar to other BC-containing particles in the LT (Cui et al., 2016; Denjean et al., 2020; D. Liu et al., 2017; Peng et al., 2016), this coating on BC through internal mixing can enhance particle absorption up to twice that of externally mixed particles (Beeler et al., 2024). Overall, measurements have demonstrated that the particle size and coating thickness of pyroCb smoke is typical larger than that of LT smoke, leading to stronger extinction and absorption.

By using measurements of coating thickness, mass concentration ratio between BC and OC, and particle size distribution (PSD), this study evaluates how particle size and coating influence the estimates of pyroCb smoke extinction, RF and stratospheric warming. The unique optical properties of coated pyroCb smoke estimated with a core-shell Mie model are applied in a global chemical transport model (CTM) and fast radiative transfer model (RTM). Although previous studies have estimated the RF of several pyroCb events, such as the 2017 Pacific Northwest Event and the 2019–2020 Australian New Year Super Outbreak event (ANYSO) (Christian et al., 2019; Das et al., 2021; Li et al., 2025; C. C. Liu et al., 2022; Sellitto et al., 2022; P. Yu et al., 2021), none of them assess the change of RF caused by the large size and coating of pyroCb smoke. Hence, focusing on 2019–2020 ANYSO event (Peterson et al., 2021), this study will advance scientific understanding of the effect of

particle size and coating of pyroCb smoke in the UTLS. Section 2 describes the data and models used in this study. Implementation of these models and simulation experiment design are introduced in Section 3. We investigate the simulation results in Section 4 and conclude the findings in Section 5.

2. Data and Model

2.1. Airborne and Satellite Measurements

Several remote sensing measurements are used in this study to characterize the unique pyroCb smoke properties and evaluate the model simulations after ANYSO injection. First, the PSD observed at New Mexico on 16 June 2022 in the DCOTSS airborne mission (Li et al., 2025) with number median radius (r_g) of 0.25 μm and geometric standard deviation (σ_g) of 1.25, comparable to volume median diameter of 0.54–0.56 μm assuming lognormal number and volume PSD, is used to parameterize pyroCb particle size (details in the supplement Text S1 and Figure S1 in Supporting Information S1).

To evalute the evolution of aerosol extinction in the UTLS simulated by CTM, the level 2 version 5.3 0.5 km resolution aerosol extinction profiles from the Stratospheric Aerosol and Gas Experiment (SAGE) III onboard the International Space Station (ISS) are analyzed, where aerosol enhancement due to ANYSO smoke injection has been identified (Kloss et al., 2021; Solomon et al., 2022; P. Yu et al., 2021). Additionally, particle size evolution can be inferred from the Angstrom Exponent (AE) profiles derived from SAGE III/ISS aerosol profiles at multiple wavelengths. When compared with CTM simulations, each sunrise/sunset event SAGE III/ISS tracked is collocated with the closest CTM spatial grid and time step (hourly) given the limited spatial and temporal samplings of SAGE III/ISS. Integrating aerosol extinction from tropopause to the TOA, the stratospheric column AOD (SAOD) from the CTM is also evaluated by SAGE III/ISS SAOD.

Lastly, the broadband radiative fluxes at TOA from the Clouds and the Earth's Radiant Energy System (CERES) spaceborne measurements are used to evaluate the RF estimates of ANYSO pyroCb smoke here. The anomaly of SW radiative flux (0.3–5 μm) after the ANYSO event is derived from level 3 Energy Balanced and Filled (EBAF) 1° × 1° Monthly mean Edition 4.1 data. Similarly, the temperature anomaly in the UTLS is derived from the Microwave Limb Sounder (MLS) measurements to further evaluate the heating caused by pyroCb smoke estimated from HR.

2.2. CTM and RTM

Equipped with the Universal tropospheric-stratospheric Chemistry eXtension (UCX) mechanism, a global three-dimensional (3D) CTM, GEOS-Chem version 13.2.1, is used to simulate the stratospheric composition perturbations after the ANYSO pyroCb injection (Eastham et al., 2014). We run GEOS-Chem at 2° × 2.5° horizontal resolution with 72 vertical layers from the surface to TOA, driven by meterology from the Modern-Era Retrospective analysis for Research and Applications, Version 2 (MERRA-2) data. Although several biomass burning emission inventories are available in GEOS-Chem, none of them consider stratospheric injection applicable for pyroCb events (Christian et al., 2019). Therefore, a new emission inventory for ANYSO pyroCb injection is developed and implemented into GEOS-Chem (Section 3.1).

Despite the availability of two aerosol microphysical schemes in GEOS-Chem (TOMAS (Trivitayanurak et al., 2008) and APM (F. Yu & Luo, 2009)), this study uses a lookup table of prescribed smoke optical properties (hereafter OP-LUT) derived from DCOTSS measurements (Section 2.1) to better isolate the effects of large particle size and thick coatings in pyroCb smoke, given the limited evaluation of stratospheric smoke PSD evolution in existing microphysical models. In each OP-LUT, mass extinction coefficient (α_{ext}), extinction efficiency (Q_{ext}), single-scattering albedo (SSA), asymmetry factor (g) and phase function (P), are provided at different wavelengths and relative humidity, in which the hygroscopic growth of hydrophilic particles and wavelength dependent refractive indices can be represented. The prescribed PSD of default smoke in GEOS-Chem was derived from ground-based measurements in North America (Latimer & Martin, 2019), which are not representative for stratospheric pyroCb.

Combining GEOS-Chem simulated stratospheric smoke concentration evolution with a fast RTM, Fu-liou model (Fu & Liou, 1992), we estimate the RF and HR caused by ANYSO smoke injection. Aerosol RF at each vertical layer is quantified by the net radiative flux (downward minus upward) difference between the scenarios where there are aerosols and where there are not. Focusing on the SW, RF and HR are computed in six wavelength bins

between 0.2 and 4 μm for each species individually before the net forcing from the smoke aerosols is assessed. Note that smoke bulk optical properties in RTM are the same as OP-LUT in GEOS-Chem.

2.3. Core-Shell Mie Model

The bulk optical properties of coated pyroCb particles through the internal mixing are simulated by a core-shell Mie model for single particle (Figure S2 in Supporting Information S1) and integrated over lognormal PSD (Ackerman & Toon, 1981; Redemann et al., 2001). OC and sulfate are assumed to be well mixed as a shell, which is then mixed internally with BC core. The densities (ρ) assumed for BC, OC and sulfate are 1.8, 1.2, and 1.7 g cm^{-3} respectively. The wavelength dependent refractive indices for the shell are volume-weighted OC and sulfate refractive indices (Eastham et al., 2014; Latimer & Martin, 2019). The lognormal PSD parameters of mixed particles (r_g) are determined by PSD of the shell and mass ratio of species consisting of core and shell, assuming constant mass and volume before and after mixing (Text S2 in Supporting Information S1). The resulting coating thickness distribution is therefore determined by the PSD (r_g) and BC mass ratio (Figure S3 in Supporting Information S1). To isolate the effect of mixing state on bulk optical properties, the external mixing assumption is applied preserving the same mass, volume and PSD (r_{g0} and r_g), where the radius of mixed particles is defined as volume-equivalent particle radius (Wang & Martin, 2007) (Text S2 in Supporting Information S1).

The left and middle columns in Figure 1 show that extinction and absorption of mixed particles exhibit similar dependencies on particle size and BC to OC mass ratio ($m_{\mathrm{BC/OC}}$) for both mixing states. α_{ext} increases with particle size, peaks at r_g of 0.2–0.3 μm, then decreases with r_g, with only weak sensitivity to $m_{\mathrm{BC/OC}}$ (Figures 1a and 1b). The coating enhances α_{ext} for small particles but reduces it for $r_g > 0.2$ μm. Overall, the change in α_{ext} due to mixing state is small (<5%) for large particles ($r_g > 0.2$ μm) (Figure 1c). SSA is primarily determined by particle size for $r_g < 0.1$ μm but dominated by $m_{\mathrm{BC/OC}}$ for larger particles (Figures 1d and 1e). The SSA difference between internal and external mixing is less than 5% and relies mainly on $m_{\mathrm{BC/OC}}$ (Figure 1f). Similarly, $m_{\mathrm{BC/OC}}$ dominates both α_{abs} and its sensitivity to mixing state (Figures 1g and 1h). However, despite the small changes in α_{ext} and SSA, coating can substantially enhance absorption, by up to 80% ($\Delta\alpha_{\mathrm{abs}}$, Figure 1i). For representative pyroCb smoke (r_g of 0.25 μm and $m_{\mathrm{BC/OC}}$ of 1.6%), coating increases α_{abs} by 50% (Figure S6 in Supporting Information S1), indicating a potentially strong enhancement of radiative warming by pyroCb smoke.

3. Methods

In this section, we describe the development of 3-D emission inventory for ANYSO pyroCb event considering the injection height and numerical experiments design for investigating the coating effect of pyroCb smoke.

3.1. 3-D pyroCb Emission Inventory Development

Based on the locations, durations, injection heights and injected aerosol mass derived using "top-down" method for the ANYSO pyroCb plumes in Peterson et al. (2021), we develop a 3-D pyroCb aerosol emission inventory considering injection height. Following Christian et al. (2019), we assume the total stratospheric aerosol mass estimated by Peterson et al. (2021) (m_{pyr}) is injected within a single model layer collocated with the observed injection heights (z_l) and an equal amount of smoke is emitted uniformly across the remaining layers from the injection height to the surface to track the simultaneous tropospheric smoke emissions (D'Angelo et al., 2022). Consequently, the hourly 1° × 1° pyroCb emission fluxes (kg·m^{-2} s^{-1}) at each model layer (F_i) are determined by Equation 1 below (Figure S4 in Supporting Information S1 shows an example):

$$F_i = \begin{cases} \dfrac{m_{\mathrm{pyr}}}{N_t \times A_1 \times N_l}, 0 \le z_i < z_l \\ \dfrac{m_{\mathrm{pyr}}}{N_t \times A_1}, z_i = z_l \end{cases}, \quad (1)$$

where z_i represents the altitude of the ith model layer and N_l is the total number of layers where $0 \le z_i < z_l$. N_t represents the total duration time of injection (unit s) and A_1 is the 1° × 1° grid box area (m^2). ANYSO emissions are temporally complex with two discontinuous injection phases: the first and largest is 29–31 December 2019, which injected total 0.2–0.8 Tg smoke into the UTLS within ~45 hr, followed by a second phase lasting over 6 hr that injected additional 0.1–0.3 Tg on 4 January 2020. Notably, in each phase, the smoke is assumed to be injected

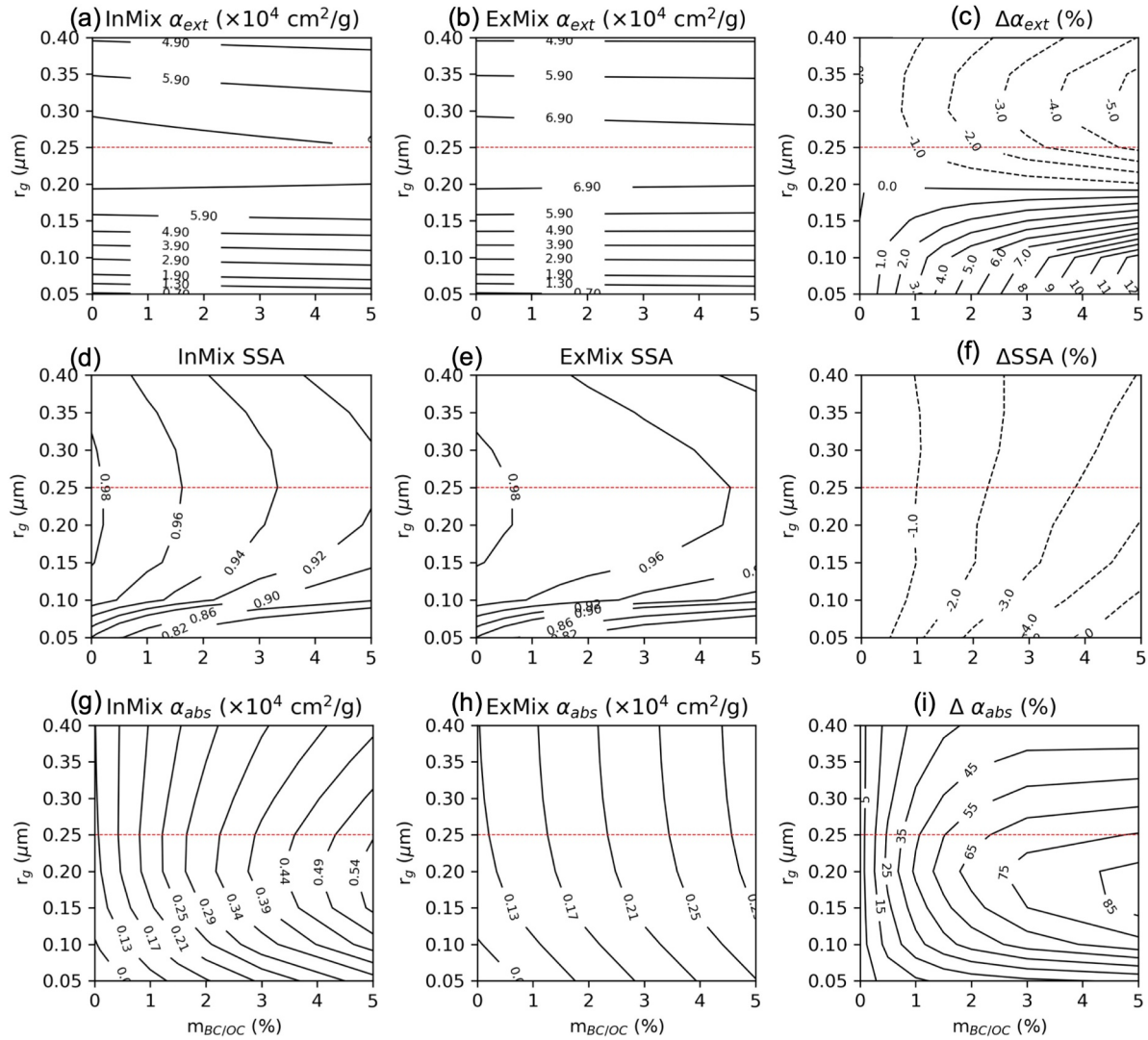

Figure 1. The variation of 550 nm α_{ext} (top row), single-scattering albedo (middle row) and α_{abs} (bottom row) for internal mixing (left column), external mixing (middle column) and their difference (InMix–ExMix, right column) as functions of r_g (the number median radius assuming a lognormal number particle size distribution (PSD)) and $m_{BC/OC}$. The geometric standard deviation of PSD (σ_g) is fixed as 1.25 and $m_{OC/SULF}$ is 1.5. For internal mixing, r_g represents the whole mixed particle radius (R_2 in Figure S2 in Supporting Information S1 for each particle); for external mixing, it is the volume-equivalent radius (Text S2 in Supporting Information S1). Red dashed lines indicate r_g = 0.25 μm, used in the GEOS-Chem simulation.

at the same rate at different locations and times. After evaluation with satellite measurements (Text S3 and Figure S5 in Supporting Information S1), a scaling factor is used in ANSYO emission inventory to inject a total of ∼1.12 Tg smoke, consistent with satellite observations. Through an extension for the Harmonized Emissions Component, this 3-D emission inventory was implemented into GEOS-Chem.

3.2. Three Sensitivity Experiments and Model Configuration

In all simulations, the GFED4 is applied to constrain the surface emission of wildfires when pyroCb injection did not occur (1–3 January 2020 and after 5 January 2020). The pyroCb smoke emission fluxes are partitioned into BC (1.6%) and OC (98.4%), based on airborne measurements (Katich et al., 2023). For BC emission, 80% is assumed as hydrophobic particles (BCPO) and 20% is hydrophilic (BCPI), while the amount of hydrophobic (OCPO) and hydrophilic OC (OCPI) particles emitted are assumed to be equal as in previous biomass burning modeling (Das et al., 2024). In all sensitivity experiments, OC from pyroCb emission is first assumed to be well mixed with background stratospheric sulfate as a OC-sulfate mixture, which is then mixed with BC either

internally or externally. Internal mixing is only applied for BCPI and OCPI, while BCPO and OCPO keeps externally mixed in all experiements.

Three experiments representing different types of smoke assuming different PSDs and mixing states in core-shell Mie model are designed (Table S1 in Supporting Information S1): (a) LT smoke: assume that smoke particles mixed by three species has small size ($r_g = 0.10$ μm, $\sigma_g = 1.25$) and BC and OC-sulfate are mixed externally; (b) ExMix pyroCb: use the same external mixing assumption as in Exp. (1) but assume large size of mixed smoke particles ($r_g = 0.25$ μm, $\sigma_g = 1.25$); (c) InMix pyroCb: assume the same large size of mixed smoke particles as in Exp. (2) but with internal mixing where BC is core. Since the size of the BC core in pyroCb smoke from in situ measurements is similar as that of coated LT smoke, all experiments use r_g of 0.02 μm for BC ($\sigma_g = 1.6$) (Beeler et al., 2024) and the same wavelength dependent refractive index of each species. Note that the mass concentrations of BC, OC and sulfate across all experiments are also the same. Generally, the comparison of Exp. (1) and Exp. (2) demonstrates the influence of the larger particle size of pyroCb smoke than LT smoke, while the impact of mixing state change can be isolated by comparing Exp. (2) and (3). Finally, another experiment named Baseline is provided as a reference for RF comparison where only surface emissions from wildfires are considered using GFED4 and the same smoke OP-LUT as in Exp. (1) is used.

4. Results

In three experiments designed above, the modeled smoke AOD and extinction profiles are compared with collocated SAGE III/ISS observations. Similar quantitative comparison is also conducted for RF and HR calculated from Fu-liou model coupled with GEOS-Chem simulations and from CERES, as well as MLS.

4.1. Coating Effect on pyroCb Smoke Extinction

Figure 2a displays that SAGE III/ISS captured enhanced aerosol extinction in the UTLS with daily SAOD at 520 nm reaching ∼0.05 after ANYSO injection compared with a background value of ∼0.01 (Figure S7 in Supporting Information S1). However, GEOS-Chem simulated SAOD is a factor of two smaller in Exp. (1) representing LT smoke (Figure 2a, blue dots), although the enhancement due to ANYSO event is still evident compared with background value. In contrast, in Exp. (2) and (3) representing large pyroCb particles (Figure 2a, red and green circles), the modeled SAOD becomes twice that in Exp. (1) and is more consistent with satellite observations. This demonstrates that if the large particle size of pyroCb smoke is not considered, the enhancement of aerosol extinction will be dramatically underestimated, consistent with estimated AOD enhancement associated with a moderate pyroCb event observed during the DCOTSS mission (Li et al., 2025). Nevertheless, there is little difference of SAOD between internally and externally mixed pyroCb smoke, in which SAOD of external mixing is ∼1% higher (pink dots showing ΔSAOD). This can be explained by only 1%–2% less mass extinction coefficient (α_{ext}) at 550 nm for internal mixing than that for external mixing at r_g of 0.25 μm representing large pyroCb particles (Figure 1c). Generally, the large particle size of pyroCb smoke compared to LT smoke is the dominant factor of much more enhanced aerosol extinction, while mixing state influences pyroCb smoke extinction little.

SAGE III/ISS aerosol extinction profiles also showcase the enhancement above the tropopause to ∼20 km (Figure 2b), exceeding 6×10^{-3} km^{-1}, far higher than the background value, which is below 5×10^{-4} km^{-1} at those altitudes. The ANYSO emission inventory we implemented in GEOS-Chem led to a successful simulation of both horizontal and vertical transport and diffusion in the pyroCb smoke plume. This is evident by a similar evolution of vertical distribution as satellite measurements caused by the movement to different latitudes of SAGE III/ISS target on Earth in different days (Figures 2b–2d). Although the underestimation of aerosol extinction in the LT smoke experiment is corrected by using the OP-LUT of large pyroCb particles, which leads to more than twice aerosol extinction (Figures 2c and 2d), the simulated aerosol extinction becomes overestimated at lower altitude, especially during the 30–50 days after ANYSO injection. Furthermore, the GEOS-Chem simulated aerosol injection is ∼2 km lower than SAGE III/ISS measurements, for which one possible reason is the absence of radiative feedback process in CTM to drive the plume self-lofting due to the light absorption and heating of BC (P. Yu et al., 2021). The uncertainty in the assumption of vertical distribution of pyroCb emission could also cause the imperfect aerosol vertical evolution simulation. Furthermore, the evolution of AE profiles from SAGE III/ISS showcases the variation of particle size with time. AE is large (1.9–2.1) during 30–50 days after the injection representing small particle size and then decreases to lower values (1.7–1.9) indicating particle size growth

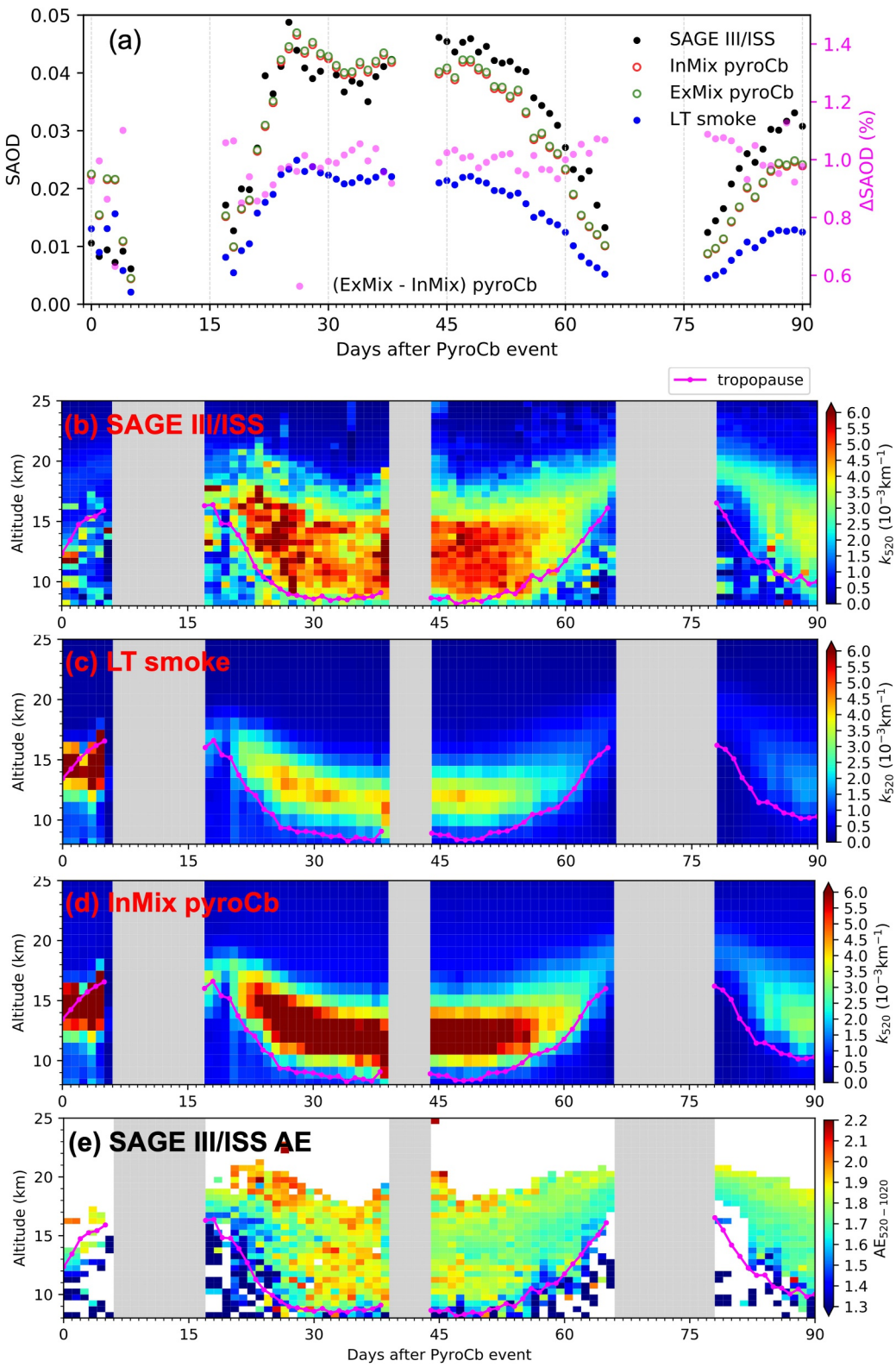

Figure 2.

(Figure 2e). This variation of particle size is not considered in the CTM yet, which could be another reason for the overestimation.

4.2. Coating Effect on RF and HR

Given the dominant non-absorbing OC in pyroCb smoke (initial $m_{BC/OC}$ is ~1.6% in the pyroCb emissions), ANYSO pyroCb smoke leads to negative SW RF at TOA, from −2.5 W/m^2 to −0.5 W/m^2 in the 1–2 months following the injection (Figure 3a, pink and green lines), comparable to the RF of volcanic sulfate from the 2008 Kasatochi eruption (Wang et al., 2013), demonstrating the significance of pyroCb smoke injection in the climate system. Furthermore, when particle size increases, both α_{ext} and SSA increase if $r_g < 0.30$ μm (Figure 1). Hence, the larger size of pyroCb smoke can lead to additional up to −0.7 W/m^2 SW RF at TOA compared to small LT smoke particles (Figure 3a, pink, green and yellow lines). In contrast, the enhanced absorption of coated pyroCb smoke compared to externally mixed pyroCb reduces this negative RF by as much as 0.1 W/m^2. CERES observed negative SW radiative flux anomaly at TOA after ANYSO injection illustrates the dominant pyroCb smoke negative RF (Figure 3b). Although the RF underestimation in the LT smoke experiment can be improved by considering larger particle size and internal mixing, demonstrated by the closer RF of internally mixed pyroCb smoke to CERES measurements, the observation is still larger than our assessment, which might result from other atmospheric composition change during this period (Figures 3c and 3d). Overall, the injection of pyroCb smoke into the UTLS can cause ~4 times stronger negative SW RF at TOA than surface only wildfire emissions (Figure 3a, gray line). Neglecting the large size of pyroCb smoke leads to a 35%–60% underestimation of RF, consistent with the enhanced radiative cooling by large pyroCb particles reported by (Li et al., 2025), whereas the enhanced absorption due to coating reduces this negative RF by only ~5%, comparable to the intrinsic uncertainty of Fu-liou fast radiative transfer approximation and thereby not significant.

The injection of pyroCb smoke from ANYSO event into the UTLS can warm the atmosphere between 12 and 18 km with HR of as high as 0.12 K/day in mid-latitude (Figure 3e). Although the SSA of particles increases for larger size, α_{ext} also increases, ultimately α_{abs} is larger (Figures 1g–1i). Consequently, the HR of stratosphere is enhanced by ~10% due to stronger mass absorption coefficient with as large as 0.016 K/day faster HR of large pyroCb smoke compared to small LT smoke particles (Figure 3f). Furthermore, the internal mixing further enhances the pyroCb smoke caused stratospheric warming by over 30% faster HR, as large as 0.03 K/day, due to the enhanced absorption caused by internal mixing (Figure 3g).

To isolate the contributions of aerosol enhancement, water vapor anomalies and dynamical variability to the MLS-observed positive temperature anomaly (ΔT), multivariable linear regression is applied following Chen et al. (2025). The fitted ΔT associated with enhanced aerosol extinction (observed by OMPS-LP) (Figure 3h, black line) closely matches the observed mid-latitude warming of up to ~3 K near 16 km after ANYSO event (Figure 3h, red line), indicating that this stratospheric warming is dominated by aerosol radiative heating. In the model, the accumulated temperature increasing derived from simulated HR of externally mixed pyroCb (Figure 3h, green line) is 0.4–0.5 K higher than that in the LT smoke experiment (Figure 3h, yellow line), but ~1 K lower than internally mixed pyroCb (Figure 3h, pink line), which agrees better with the observed ΔT in the first 2 months after ANYSO injection. Generally, the coating of large pyroCb smoke particles results in twice the heating in the UTLS compared with that caused by particle size growth alone. The underestimation of temperature increasing assuming externally mixed pyroCb smoke compared with satellite measurements demonstrates the significance to consider the coating of pyroCb smoke when evaluating pyroCb caused stratospheric warming.

5. Conclusions and Discussions

With the goal of assessing the large size and coating of pyroCb smoke particles on aerosol extinction, RF and HR, we developed a three-dimensional emission inventory for pyroCb smoke from 2019 to 2020 Australian megafires (ANYSO) that incorporates injection height measurements from previous studies. This inventory was

Figure 2. The comparison of daily SAOD (a) and aerosol extinction coefficient profile (b)–(d) at 520 nm averaged in 20°S–70°S among three experiments and Stratospheric Aerosol and Gas Experiment (SAGE) III/International Space Station (ISS) measurements after ANYSO injection (4 January 2020). The Angstrom Exponent profiles calculated from SAGE III/ISS aerosol extinction between 520 and 1,020 nm are in (e). The model simulations are collocated with each SAGE III/ISS event before averaged. Pink dots in (a) showcase the relative difference of SAOD between Exp. (2) and (3). Modeled SAOD is accumulated by aerosol optical depth in each layer from the tropopause defined by MERRA-2 to top-of-atmosphere, shown as the magenta dotted lines in (b)–(e).

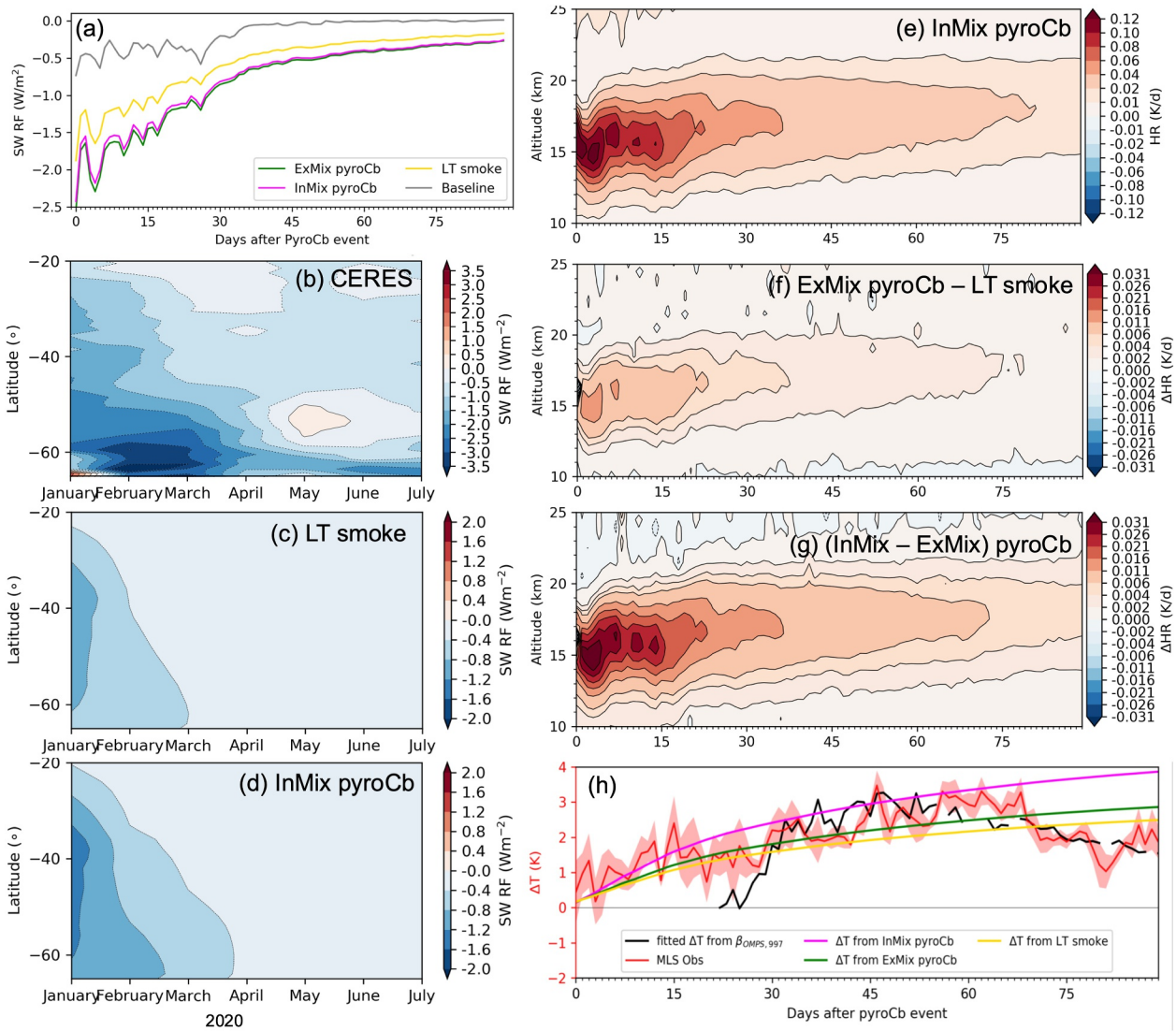

Figure 3. The comparison of daily clear sky shortwave (SW) radiative forcing at top of the atmosphere (TOA) averaged in 35°–45°S among different experiments estimated by Fu-liou model (a), as well as monthly zonal mean estimates ((c) for lower troposphere smoke and (d) for InMix pyroCb) compared with Clouds and the Earth's Radiant Energy System observed TOA SW radiative flux anomaly (b). Daily heating rate (HR) profile at 10–25 km in InMix pyroCb experiment (e) and HR differences (ΔHR) among different experiments are also averaged in 35°–45°S (f) and (g). In (h), Microwave Limb Sounder observed temperature anomaly (red line) is compared with multivariate linear fitting from OMPS-LP observed aerosol extinction profile at 997 nm (black line), and temperature increasing caused by smoke heating estimated in different experiments.

implemented into the GEOS-Chem to simulate the evolution of pyroCb smoke in the UTLS. Coupling GEOS-Chem with Fu-Liou RTM, we estimated the RF and HR associated with ANYSO pyroCb smoke. The isolation of effect from large particle size and coating through internal mixing is achieved by comparing the results from three sensitivity experiments with different particle size and mixing state assumptions.

While conserving the mass and volume of each species, internal mixing was found to enhance the absorption efficiency (lower SSA) compared to external mixing, whereas the mass extinction coefficient is reduced for large particles (~0.25 μm r_g). Consequently, we found that the larger size of pyroCb smoke particles compared with typical lower tropospheric smoke (<0.1 μm r_g) can double the smoke extinction and AOD (SAOD), which aligns with the strong aerosol extinction enhancements observed by SAGE III/ISS. However, changes in mixing state have minimal impact on SAOD for these large pyroCb particles. Applied into RTM, the unique microphysics of coated pyroCb smoke can lead to 35%–60% stronger SW RF at TOA, primarily resulting from the larger particle size, while the internal mixing results in ~5% reduction of SW RF than external mixing. Coating can enhance

stratospheric heating by 1–1.5K in the UTLS, twice the enhancement of increasing particle size alone, which agrees with MLS observations.

Although our simulated SAOD, RF and HR for ANYSO pyroCb smoke agree better with satellite observations after incorporating the effect of the larger particle size and internal mixing, model deficiencies still remain in aerosol extinction profiles and RF under the assumption of fixed particle size. Therefore, observations of particle size profile and its evolution with plume age are essential to better constrain the pyroCb smoke distribution and associated RF in the future, especially from satellite instruments with long-term stable measurements. The performance of bimodal PSD assumptions and aerosol microphysics-based models such as GEOS-Chem APM for simulating aged pyroCb smoke and its long-term climate impacts warrants further investigation in the future. The assumption of pyroCb smoke emission profile also influences the smoke evolution simulation and RF, which requires more evidences from observations to support. Furthermore, the influence of particle size and mixing state of pyroCb smoke may influence smoke catalyzed heteorogenous reactions in the UTLS by modifying the particle surface area density and composition, which should be investigated in the future.

Conflict of Interest

The authors declare no conflicts of interest relevant to this study.

Availability Statement

The coated pyroCb smoke optical properties derived from core-shell Mie model assuming external or internal mixing are available at zenodo via https://doi.org/10.5281/zenodo.16956369 (Chen, 2025a) with Creative Commons Attribution 4.0 International license. The SAGE III/ISS observed aerosol extinction profile and SAOD, their counterparts from collocated GEOS-Chem simulation, the SW flux anomaly observed by CERES and Fu-liou model simulated ANYSO pyroCb smoke RF and HR are also opened at zenodo via the same link. The python codes used to process satellite and model data, as well as make plots are all preserved at https://doi.org/10.5281/zenodo.17049609 (Chen, 2025b), available via open access.

Acknowledgments
This work was supported by the funding from National Aeronautics and Space Administration (NASA), Stratospheric Aerosol and Gas Experiment III/ International Space Station program (SAGE III/ISS, Grant 80NSSC21K1199 and 80NSSC25K7183). We acknowledge the NASA satellite missions, including the OMPS-LP, SAGE III/ISS, and MLS teams, for providing stratospheric gases and aerosol products. Support for D. P. was provided by the U. S. Naval Research Laboratory's 6.2 Base Program, NASA's Modeling, Analysis, and Prediction (MAP) Program (80HQTR21T0099), FireSense Program, and INjected Smoke and PYRocumulonimbus Experiment (INSPYRE). Y.L., F.K., and J.D. acknowledge support from NASA under DCOTSS award (80NSSC19K0326). Y. L. also acknowledges partial support from the NOAA Climate & Global Change Postdoctoral Fellowship Program (award NA23OAR4310383B).

References

Ackerman, T. P., & Toon, O. B. (1981). Absorption of visible radiation in atmosphere containing mixtures of absorbing and nonabsorbing particles. *Applied Optics*, *20*(20), 3661–3668. https://doi.org/10.1364/AO.20.003661

Alonso-Blanco, E., Calvo, A. I., Fraile, R., & Castro, A. (2012). The influence of wildfires on aerosol size distributions in rural areas. *The Scientific World Journal*, *13*(1), 735697. https://doi.org/10.1100/2012/735697

Andersson, S. M., Martinsson, B. G., Vernier, J.-P., Friberg, J., Brenninkmeijer, C. A., Hermann, M., et al. (2015). Significant radiative impact of volcanic aerosol in the lowermost stratosphere. *Nature Communications*, *6*(1), 1–8. https://doi.org/10.1038/ncomms8692

Beeler, P., Kumar, J., Schwarz, J. P., Adachi, K., Fierce, L., Perring, A. E., et al. (2024). Light absorption enhancement of black carbon in a pyrocumulonimbus cloud. *Nature Communications*, *15*(1), 6243. https://doi.org/10.1038/s41467-024-50070-0

Chen, X. (2025a). Particle coating influences pyrocumulonimbus smoke radiative forcing and stratospheric warming: Insights from 2019-2020 Australian megafires [Dataset]. *Zenodo*. https://doi.org/10.5281/zenodo.16956369

Chen, X. (2025b). xchen224/PyroCb_GC_published: Initial release (v0.0.1) [Software]. *Zenodo*. https://doi.org/10.5281/zenodo.17049609

Chen, X., Wang, J., Zhou, M., Lu, Z., Jaegle, L., Oman, L. D., & Taha, G. (2025). Impact of water vapor on stratospheric temperature after the 2022 Hunga Tonga eruption: Direct radiative cooling versus indirect warming by facilitating large particle formation. *npj Climate and Atmospheric Science*, *8*(1), 192. https://doi.org/10.1038/s41612-025-01056-2

Christian, K., Wang, J., Ge, C., Peterson, D., Hyer, E., Yorks, J., & McGill, M. (2019). Radiative forcing and stratospheric warming of pyrocumulonimbus smoke aerosols: First modeling results with multisensor (EPIC, CALIPSO, and CATS) views from space. *Geophysical Research Letters*, *46*(16), 10061–10071. https://doi.org/10.1029/2019GL082360

Cui, X., Wang, X., Yang, L., Chen, B., Chen, J., Andersson, A., & Gustafsson, Ö. (2016). Radiative absorption enhancement from coatings on black carbon aerosols. *Science of The Total Environment*, *551–552*, 51–56. https://doi.org/10.1016/j.scitotenv.2016.02.026

Dahlkötter, F., Gysel, M., Sauer, D., Minikin, A., Baumann, R., Seifert, P., et al. (2014). The Pagami creek smoke plume after long-range transport to the upper troposphere over Europe – Aerosol properties and black carbon mixing state. *Atmospheric Chemistry and Physics*, *14*(12), 6111–6137. https://doi.org/10.5194/acp-14-6111-2014

D'Angelo, G., Guimond, S., Reisner, J., Peterson, D. A., & Dubey, M. (2022). Contrasting stratospheric smoke mass and lifetime from 2017 Canadian and 2019/2020 Australian megafires: Global simulations and satellite observations. *Journal of Geophysical Research: Atmospheres*, *127*(10), e2021JD036249. https://doi.org/10.1029/2021JD036249

Das, S., Colarco, P. R., Bian, H., & Gassó, S. (2024). Improved simulations of biomass burning aerosol optical properties and lifetimes in the NASA GEOS model during the ORACLES-I campaign. *Atmospheric Chemistry and Physics*, *24*(7), 4421–4449. https://doi.org/10.5194/acp-24-4421-2024

Das, S., Colarco, P. R., Oman, L. D., Taha, G., & Torres, O. (2021). The long-term transport and radiative impacts of the 2017 British Columbia pyrocumulonimbus smoke aerosols in the stratosphere. *Atmospheric Chemistry and Physics*, *21*(15), 12069–12090. https://doi.org/10.5194/acp-21-12069-2021

Denjean, C., Brito, J., Libois, Q., Mallet, M., Bourrianne, T., Burnet, F., et al. (2020). Unexpected biomass burning aerosol absorption enhancement explained by black carbon mixing State. *Geophysical Research Letters*, *47*(19), e2020GL089055. https://doi.org/10.1029/2020GL089055

Eastham, S. D., Weisenstein, D. K., & Barrett, S. R. H. (2014). Development and evaluation of the unified tropospheric–stratospheric chemistry extension (UCX) for the global chemistry-transport model GEOS-chem. *Atmospheric Environment*, *89*, 52–63. https://doi.org/10.1016/j.atmosenv.2014.02.001

Fromm, M., Alfred, J., Hoppel, K., Hornstein, J., Bevilacqua, R., Shettle, E., et al. (2000). Observations of boreal forest fire smoke in the stratosphere by POAM III, SAGE II, and LiDAR in 1998. *Geophysical Research Letters*, *27*(9), 1407–1410. https://doi.org/10.1029/1999GL011200

Fromm, M. D., & Servranckx, R. (2003). Transport of forest fire smoke above the tropopause by supercell convection. *Geophysical Research Letters*, *30*(10). https://doi.org/10.1029/2002GL016820

Fu, Q., & Liou, K. N. (1992). On the correlated k-Distribution method for radiative transfer in nonhomogeneous atmospheres. *Journal of the Atmospheric Sciences*, *49*(22), 2139–2156. https://doi.org/10.1175/1520-0469(1992)049<2139:OTCDMF>2.0.CO;2

Ge, C., Wang, J., Carn, S., Yang, K., Ginoux, P., & Krotkov, N. (2016). Satellite-based global volcanic SO2 emissions and sulfate direct radiative forcing during 2005–2012. *Journal of Geophysical Research: Atmospheres*, *121*(7), 3446–3464. https://doi.org/10.1002/2015jd023134

Heinold, B., Baars, H., Barja, B., Christensen, M., Kubin, A., Ohneiser, K., et al. (2022). Important role of stratospheric injection height for the distribution and radiative forcing of smoke aerosol from the 2019–2020 Australian wildfires. *Atmospheric Chemistry and Physics*, *22*(15), 9969–9985. https://doi.org/10.5194/acp-22-9969-2022

Jacobson, M. Z. (2001). Strong radiative heating due to the mixing state of black carbon in atmospheric aerosols. *Nature*, *409*(6821), 695–697. https://doi.org/10.1038/35055518

Katich, J., Apel, E., Bourgeois, I., Brock, C., Bui, T., Campuzano-Jost, P., et al. (2023). Pyrocumulonimbus affect average stratospheric aerosol composition. *Science*, *379*(6634), 815–820. https://doi.org/10.1126/science.add3101

Kloss, C., Sellitto, P., von Hobe, M., Berthet, G., Smale, D., Krysztofiak, G., et al. (2021). Australian Fires 2019–2020: Tropospheric and Stratospheric Pollution Throughout the Whole Fire Season [Original Research]. *Frontiers in Environmental Science*, *9*, 652024. https://doi.org/10.3389/fenvs.2021.652024

Lack, D. A., Langridge, J. M., Bahreini, R., Cappa, C. D., Middlebrook, A. M., & Schwarz, J. P. (2012). Brown carbon and internal mixing in biomass burning particles. *Proceedings of the National Academy of Sciences of the United States of America*, *109*(37), 14802–14807. https://doi.org/10.1073/pnas.1206575109

Latimer, R. N. C., & Martin, R. V. (2019). Interpretation of measured aerosol mass scattering efficiency over North America using a chemical transport model. *Atmospheric Chemistry and Physics*, *19*(4), 2635–2653. https://doi.org/10.5194/acp-19-2635-2019

Li, Y., Dykema, J., Deshler, T., & Keutsch, F. (2021). Composition dependence of stratospheric aerosol shortwave radiative forcing in northern midlatitudes. *Geophysical Research Letters*, *48*(24), e2021GL094427. https://doi.org/10.1029/2021GL094427

Li, Y., Dykema, J. A., Peterson, D. A., Feng, X., Shen, X., June, N. A., et al. (2025). Enhanced radiative cooling by large aerosol particles from wildfire-driven thunderstorms. *Science Advances*, *11*(50), eadw6526. https://doi.org/10.1126/sciadv.adw6526

Liu, C. C., Portmann, R. W., Liu, S., Rosenlof, K. H., Peng, Y., & Yu, P. (2022). Significant effective radiative forcing of stratospheric wildfire smoke. *Geophysical Research Letters*, *49*(17), e2022GL100175. https://doi.org/10.1029/2022gl100175

Liu, D., Whitehead, J., Alfarra, M. R., Reyes-Villegas, E., Spracklen, D. V., Reddington, C. L., et al. (2017). Black-carbon absorption enhancement in the atmosphere determined by particle mixing state. *Nature Geoscience*, *10*(3), 184–188. https://doi.org/10.1038/ngeo2901

Martins, J. V., Artaxo, P., Liousse, C., Reid, J. S., Hobbs, P. V., & Kaufman, Y. J. (1998). Effects of black carbon content, particle size, and mixing on light absorption by aerosols from biomass burning in Brazil. *Journal of Geophysical Research*, *103*(D24), 32041–32050. https://doi.org/10.1029/98jd02593

Peng, J., Hu, M., Guo, S., Du, Z., Zheng, J., Shang, D., et al. (2016). Markedly enhanced absorption and direct radiative forcing of black carbon under polluted urban environments. *Proceedings of the National Academy of Sciences*, *113*(16), 4266–4271. https://doi.org/10.1073/pnas.1602310113

Peterson, D. A., Campbell, J. R., Hyer, E. J., Fromm, M. D., Kablick, G. P., Cossuth, J. H., & DeLand, M. T. (2018). Wildfire-driven thunderstorms cause a volcano-like stratospheric injection of smoke. *npj Climate and Atmospheric Science*, *1*, 30. https://doi.org/10.1038/s41612-018-0039-3

Peterson, D. A., Fromm, M. D., McRae, R. H., Campbell, J. R., Hyer, E. J., Taha, G., et al. (2021). Australia's black summer pyrocumulonimbus super outbreak reveals potential for increasingly extreme stratospheric smoke events. *npj Climate and Atmospheric Science*, *4*(1), 1–16. https://doi.org/10.1038/s41612-021-00192-9

Peterson, D. A., Hyer, E. J., Campbell, J. R., Solbrig, J. E., & Fromm, M. D. (2017). A conceptual model for development of intense pyrocumulonimbus in western North America. *Monthly Weather Review*, *145*(6), 2235–2255. https://doi.org/10.1175/mwr-d-16-0232.1

Peterson, D. A., Thapa, L. H., Saide, P. E., Soja, A. J., Gargulinski, E. M., Hyer, E. J., et al. (2022). Measurements from inside a thunderstorm driven by wildfire: The 2019 FIREX-AQ feld experiment. *Bulletin of the American Meteorological Society*, *103*(9), E2140–E2167. https://doi.org/10.1175/BAMS-D-21-0049.1

Portin, H., Mielonen, T., Leskinen, A., Arola, A., Pärjälä, E., Romakkaniemi, S., et al. (2012). Biomass burning aerosols observed in Eastern Finland during the Russian wildfires in summer 2010 – Part 1: In-situ aerosol characterization. *Atmospheric Environment*, *47*, 269–278. https://doi.org/10.1016/j.atmosenv.2011.10.067

Redemann, J., Russell, P. B., & Hamill, P. (2001). Dependence of aerosol light absorption and single-scattering albedo on ambient relative humidity for sulfate aerosols with black carbon cores. *Journal of Geophysical Research*, *106*(D21), 27485–27495. https://doi.org/10.1029/2001JD900231

Reid, J. S., Eck, T. F., Christopher, S. A., Koppmann, R., Dubovik, O., Eleuterio, D. P., et al. (2005). A review of biomass burning emissions part III: Intensive optical properties of biomass burning particles. *Atmospheric Chemistry and Physics*, *5*(3), 827–849. https://doi.org/10.5194/acp-5-827-2005

Reid, J. S., & Hobbs, P. V. (1998). Physical and optical properties of young smoke from individual biomass fires in Brazil. *Journal of Geophysical Research*, *103*(D24), 32013–32030. https://doi.org/10.1029/98jd00159

Ridley, D. A., Solomon, S., Barnes, J. E., Burlakov, V. D., Deshler, T., Dolgii, S. I., et al. (2014). Total volcanic stratospheric aerosol optical depths and implications for global climate change. *Geophysical Research Letters*, *41*(22), 7763–7769. https://doi.org/10.1002/2014GL061541

Robock, A. (2000). Volcanic eruptions and climate. *Reviews of Geophysics*, *38*(2), 191–219. https://doi.org/10.1029/1998rg000054

Sellitto, P., Belhadji, R., Kloss, C., & Legras, B. (2022). Radiative impacts of the Australian bushfires 2019–2020 – Part 1: Large-scale radiative forcing. *Atmospheric Chemistry and Physics*, *22*(14), 9299–9311. https://doi.org/10.5194/acp-22-9299-2022

Solomon, S., Daniel, J. S., Neely, R. R., Vernier, J.-P., Dutton, E. G., & Thomason, L. W. (2011). The persistently variable "background" stratospheric aerosol layer and global climate change. *Science*, *333*(6044), 866–870. https://doi.org/10.1126/science.1206027

Solomon, S., Dube, K., Stone, K., Yu, P., Kinnison, D., Toon, O. B., et al. (2022). On the stratospheric chemistry of midlatitude wildfire smoke. *Proceedings of the National Academy of Sciences of the United States of America*, *119*(10), e2117325119. https://doi.org/10.1073/pnas.2117325119

Taylor, J. W., Wu, H., Szpek, K., Bower, K., Crawford, I., Flynn, M. J., et al. (2020). Absorption closure in highly aged biomass burning smoke. *Atmospheric Chemistry and Physics*, *20*(19), 11201–11221. https://doi.org/10.5194/acp-20-11201-2020

Trivitayanurak, W., Adams, P. J., Spracklen, D. V., & Carslaw, K. S. (2008). Tropospheric aerosol microphysics simulation with assimilated meteorology: Model description and intermodel comparison. *Atmospheric Chemistry and Physics*, *8*(12), 3149–3168. https://doi.org/10.5194/acp-8-3149-2008

Wang, J., & Christopher, S. A. (2006). Mesoscale modeling of Central American smoke transport to the United States: 2. Smoke radiative impact on regional surface energy budget and boundary layer evolution. *Journal of Geophysical Research*, *111*(D14). https://doi.org/10.1029/2005JD006720

Wang, J., Christopher, S. A., Nair, U. S., Reid, J. S., Prins, E. M., Szykman, J., & Hand, J. L. (2006). Mesoscale modeling of Central American smoke transport to the United States: 1. "Top-down" assessment of emission strength and diurnal variation impacts. *Journal of Geophysical Research*, *111*(D5). https://doi.org/10.1029/2005JD006416

Wang, J., & Martin, S. T. (2007). Satellite characterization of urban aerosols: Importance of including hygroscopicity and mixing state in the retrieval algorithms. *Journal of Geophysical Research*, *112*(D17). https://doi.org/10.1029/2006jd008078

Wang, J., Park, S., Zeng, J., Ge, C., Yang, K., Carn, S., et al. (2013). Modeling of 2008 Kasatochi volcanic sulfate direct radiative forcing: Assimilation of OMI SO_2 plume height data and comparison with MODIS and CALIOP observations. *Atmospheric Chemistry and Physics*, *13*(4), 1895–1912. https://doi.org/10.5194/acp-13-1895-2013

Yu, F., & Luo, G. (2009). Simulation of particle size distribution with a global aerosol model: Contribution of nucleation to aerosol and CCN number concentrations. *Atmospheric Chemistry and Physics*, *9*(20), 7691–7710. https://doi.org/10.5194/acp-9-7691-2009

Yu, P., Davis, S. M., Toon, O. B., Portmann, R. W., Bardeen, C. G., Barnes, J. E., et al. (2021). Persistent stratospheric warming due to 2019–2020 Australian wildfire smoke. *Geophysical Research Letters*, *48*(7), e2021GL092609. https://doi.org/10.1029/2021gl092609

References From the Supporting Information

Andreae, M. O. (2019). Emission of trace gases and aerosols from biomass burning – An updated assessment. *Atmospheric Chemistry and Physics*, *19*(13), 8523–8546. https://doi.org/10.5194/acp-19-8523-2019

Pumphrey, H. C., Read, W. G., Livesey, N. J., & Yang, K. (2015). Observations of volcanic SO2 from MLS on Aura. *Atmospheric Measurement Techniques*, *8*(1), 195–209. https://doi.org/10.5194/amt-8-195-2015

Seinfeld, J. H., & Pandis, S. N. (2016). *Atmospheric chemistry and physics: From air pollution to climate change* (3rd ed.). John Wiley & Sons.